Supporting Information

Ultra-Superior High-Temperature Energy Storage Properties in Polymer Nanocomposites via Rational Design of Core-Shell Structured Inorganic Antiferroelectric Fillers

Zhenhao Fan [a,b], Shuaibing Gao [a], Yunfei Chang [b,*], Dawei Wang [b], Xin Zhang [c], Haitao Huang [d,*], Yunbin He [a,*], Qingfeng Zhang [a,*]

[a]*School of Materials Science & Engineering, Hubei University, Wuhan 430062, China*

[b]*School of Instrumentation Science and Engineering, Harbin Institute of Technology, Harbin 150080, China*

[c]*State Key Laboratory of Advanced Technology for Materials Synthesis and Processing, Wuhan University of Technology, Wuhan 430070, China*

[d]*Department of Applied Physics, The Hong Kong Polytechnic University, Hong Kong, China*

[*]Corresponding authors.
E-mail addresses: changyunfei@hit.edu.cn (Y. Chang), aphhuang@polyu.edu.hk (H. Huang), ybhe@hubu.edu.cn (Y. He), zhangqingfeng@hubu.edu.cn (Q. Zhang)

Experimental

Preparation of PLZST AFE nanoparticles and ceramics: $(Pb_{0.955}La_{0.03})(Zr_{0.50}Sn_{0.42}Ti_{0.08})O_3$ AFE nanoparticles and ceramics with excess 1 wt.% PbO content were prepared by the solid-state reaction method. PbO, TiO_2, ZrO_2, SnO_2, and La_2O_3 with purities higher than 98% were used as raw materials and weighed according to above stoichiometric formula. The powders were ball milled for 4 h and then calcined at 870 °C for 2 h in air. After re-milling for 8 h, the obtained nanoparticles were pressed into discs and sintered at 1230 °C for 3 h to fabricate the ceramics. Silver electrodes were pasted onto both sides of the polished ceramics and fired at 550 °C for 10 min to measure the electrical properties.

Fabrication of the core-shell structured PLZST@Al_2O_3 AFE nanoparticles:Al_2O_3 sol was prepared by the sol-gel method. Firstly, 0.02 M aluminum isopropyl alcohol was added into 50 mL ethylene glycol diethyl ether, and stirred until it was completely dissolved. After that, 0.02 M acetyl acetone and 10 mL acetic acid were added and stirred to obtain pure Al_2O_3 sol. In the following, according to the weight ratio of Al_2O_3 : PLZST = 1 : 20, appropriate amount of Al_2O_3 sol and PLZST NPs were mixed, grinded, and calcined at 600 °C for 2 h to obtain core-shell structured PLZST@Al_2O_3 AFE nanoparticles.

Fabrication of PLZST/PEI and PLZST@Al_2O_3/PEI nanocomposites: PEI nanocomposites with different contents of PLZST@Al_2O_3 NPs were prepared by a typical solution casting method. The PEI polymers were first dissolved in N-methyl pyrrolidone (NMP) solvent and heated at 50 °C for 2 h to obtain transparent PEI

solution. At the same time, the PLZST@Al_2O_3NPs were also dispersed in NMP solvent by ultrasonically stirring for 20 min. Then, the above two solutions were mixed together and stirred for 12 h at room temperature to realize uniform dispersion of NPs. In the following, the mixed solution was cast onto a clean glass substrate, and dried at 60 °C for 12 h in vacuum to volatilize NMP. After drying, the nanocomposites with a thickness of about 9-12 μm were stripped from the glass substrate, and covered with Au electrodes with the diameter of 2 mm.

Characterization: The crystal structure of the nanocomposites was examined by the D8 Advance X-ray diffraction (XRD, Bruker, Germany). The infrared spectrum was evaluated by the Nicolet iS50 Fourier transform infrared spectroscopy (FT-IR, Thermo Fisher Scientific, USA). The scanning transmission electron microscopy (STEM)-energy dispersive spectroscopy (EDS) mapping and EDS line-scanning images were tested by transmission electron microscopy (TEM, Talos F200X, FEI, USA). The glass transition temperature and specific heat capacity were recorded with the 200 F3 Maia differential scanning calorimetry (DSC, Netzsch, Germany) at a heating rate of 10 °C min^{-1} under nitrogen atmosphere. The thermal decomposition temperatures were measured by the TGA1 thermogravimetric analysis (TGA, Mettler Toledo, Switzerland) at a heating rate of 10 °C min^{-1} under air atmosphere. The surface morphology and the element distribution were observed by the SIGMA 500field-emission scanning electron microscopy (FESEM, Germany). The thermal diffusivity is measured by the LFA 467 HyperFlash system (NETZSCH, Germany). The thermal conductivity of PLZST NPs, and PLZST/PEI and PLZST@Al_2O_3

nanocomposites is acquired according to their specific heat, thermal diffusivity and density. The dielectric constant and loss were obtained by the TH 2827A precision LCR meter (Tonghui Electronic Co., Ltd., China). The E_b was achieved by using the NJC5010 withstand voltage tester (Gogo Instruments Technology, China). The thermally stimulated depolarization currents (TSDC) tests were measured by the PCTS-2500 pyroelectric test system (Yanhe Technology, China). The *D-E* loops, leakage current and resistivity at different temperatures and electric fields, and current-electric field (*I-E*) curves were acquired by the Precision LC II ferroelectric testing system (Radiant Technologies Inc., USA). The energy storage performances were calculated from above *D-E* loops.The E_g and E_a of PLZST materials were achieved by the UV-3600 Plus UV-Vis-NIR spectrophotometer (Shimadzu, Japan) and Escalab 250Xi Ultraviolet photoelectron spectroscopy (UPS) with the He-I lamp radiation (21.2 eV) (Thermo Scientific, USA)

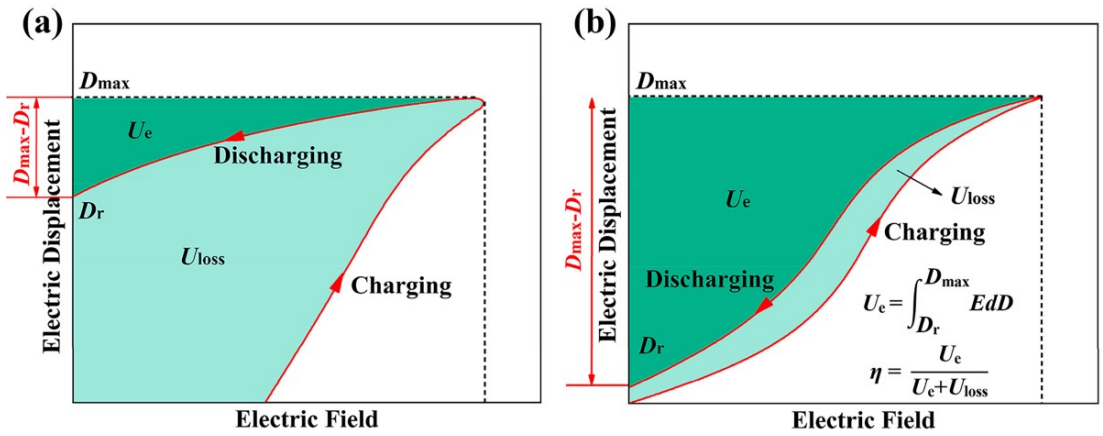

Fig. S1. *D-E* loops and energy storage behavior of (a) ferroelectrics and (b) antiferroelectrics.

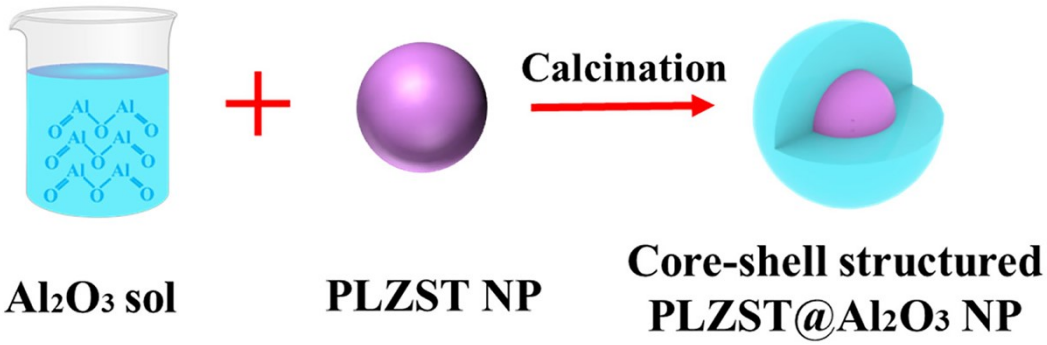

Fig. S2. Schematic diagram of preparing core-shell structured PLZST@Al_2O_3 NPs.

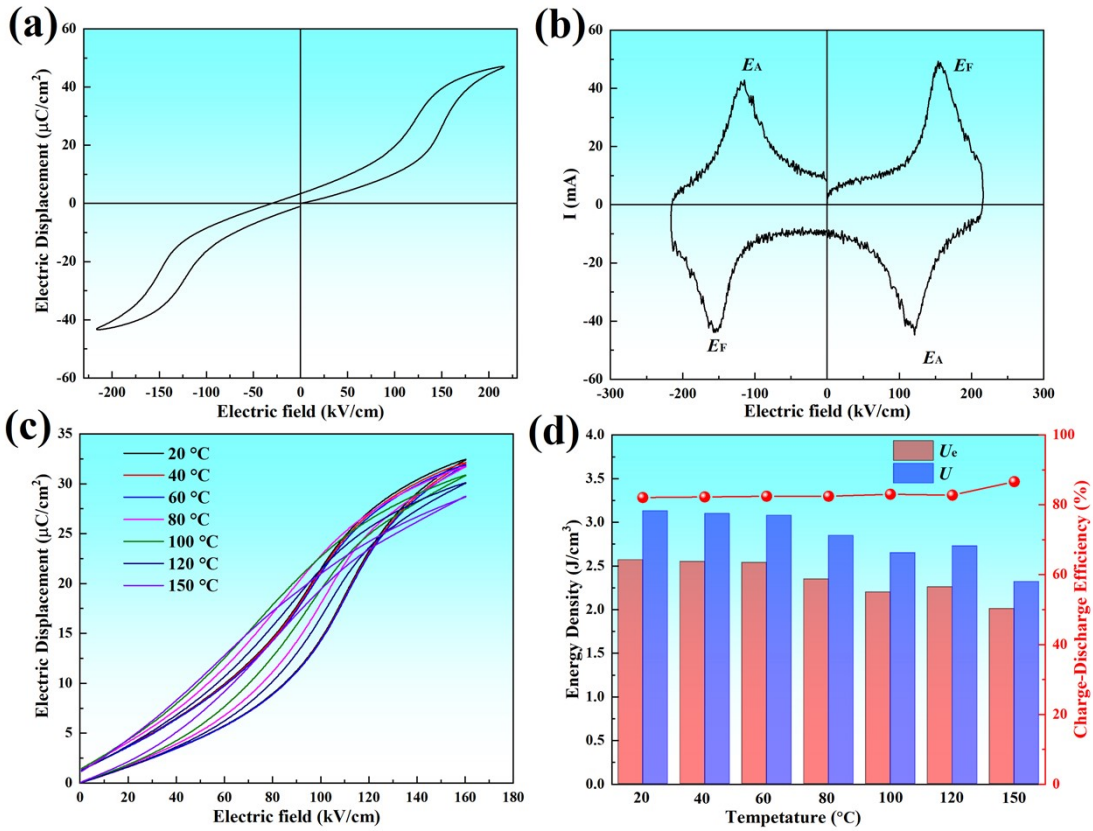

Fig. S3. (a) The double *D-E* loop and (b) the corresponding *I-E* curve of the PLZST ceramic. (c) Unipolar *D-E* loops and (d) energy storage properties of the PLZST ceramic from 20 to 150 °C.

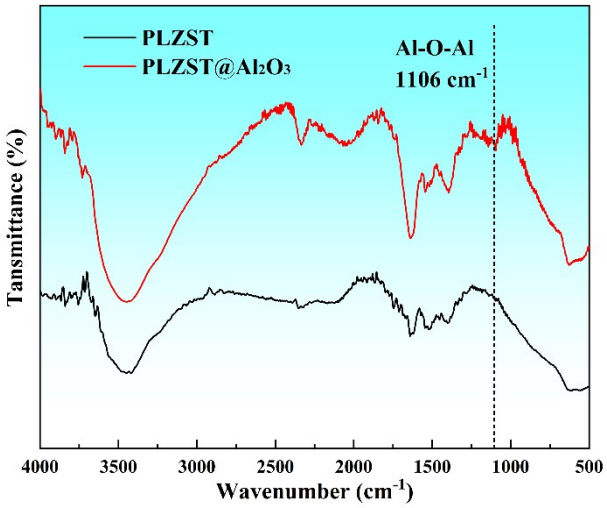

Fig. S4. Fourier transform infrared spectroscopy of PLZST and PLZST@Al_2O_3 NPs.

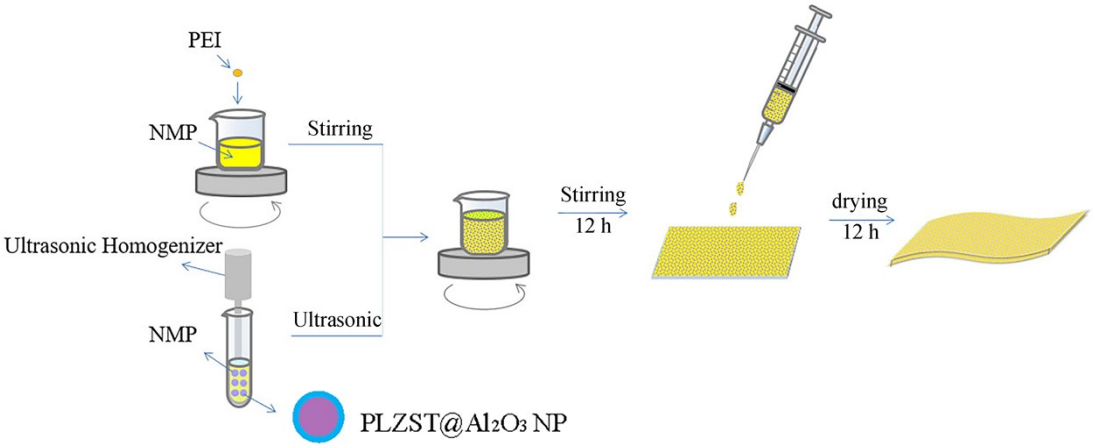

Fig. S5. Schematic illustration of preparation process of PLZST@Al_2O_3 NPs/PEI nanocomposites.

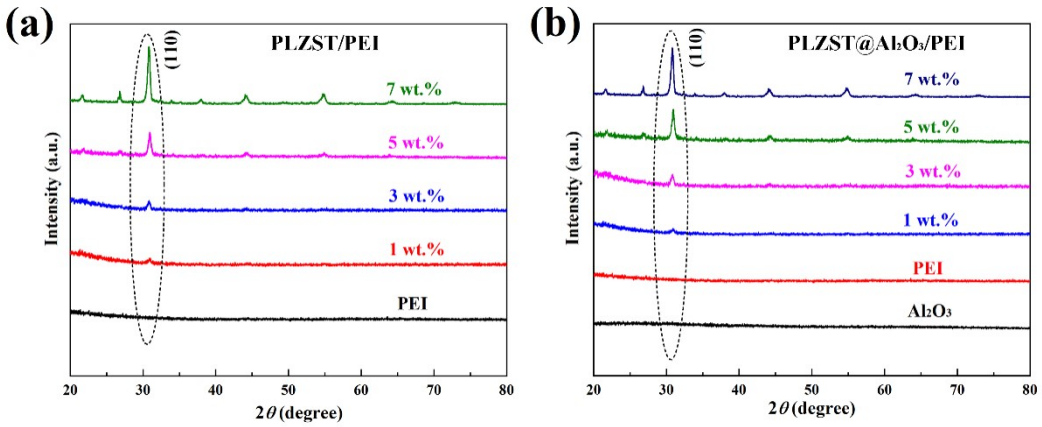

Fig. S6. XRD patterns of PEI nanocomposites filled with various (a) PLZST and (b) PLZST@Al_2O_3 NP contents. The XRD pattern of Al_2O_3 nanopowders prepared by sol-gel method.

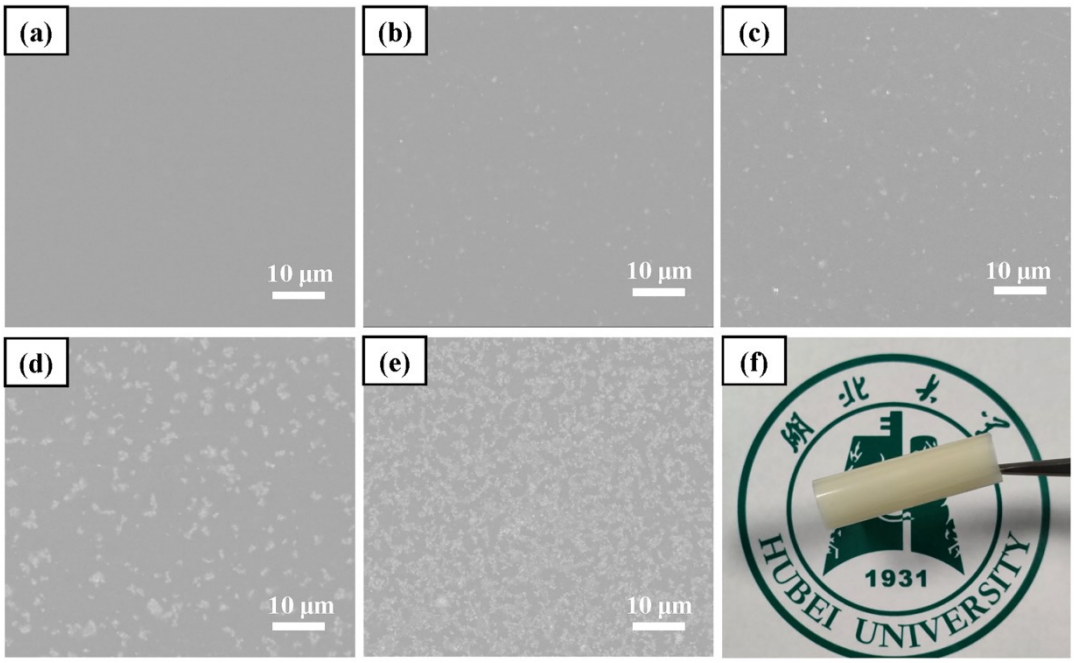

Fig. S7. Surface FESEM images of PEI nanocomposites containing (a) 0 wt.%, (b) 1 wt.%, (c) 3 wt.%, (d) 5 wt.%, (e) 7 wt.% PLZST@Al_2O_3 NPs. (f) Macroscopic digital photograph of the flexible PEI nanocomposite containing 3 wt.% PLZST@Al_2O_3 NPs.

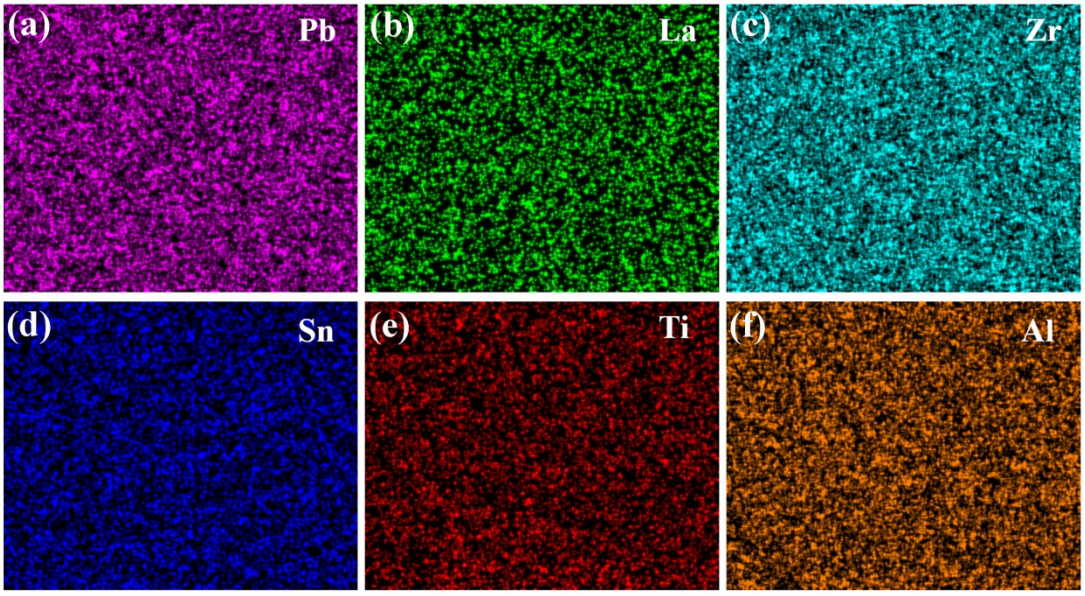

Fig. S8. Elemental mapping images of (a) Pb, (b) La, (c) Zr, (d) Sn, (e) Ti and (f) Al of the PEI nanocomposite loaded with 3 wt.% PLZST@Al_2O_3 NPs.

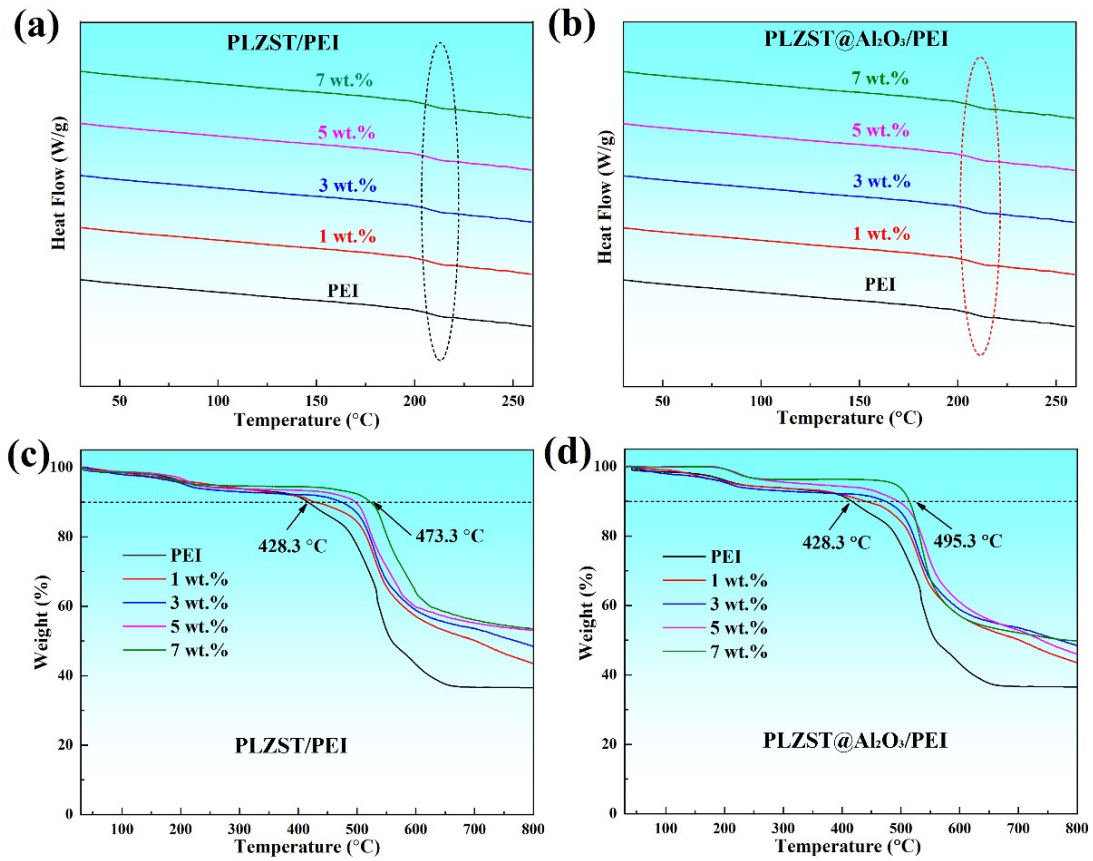

Fig. S9. Differential scanning calorimetry of PEI nanocomposites loaded with various (a) PLZST and (b) PLZST@Al_2O_3 contents. Thermogravimetric analysis of PEI nanocomposites loaded with various (c) PLZST and (d) PLZST@Al_2O_3 contents.

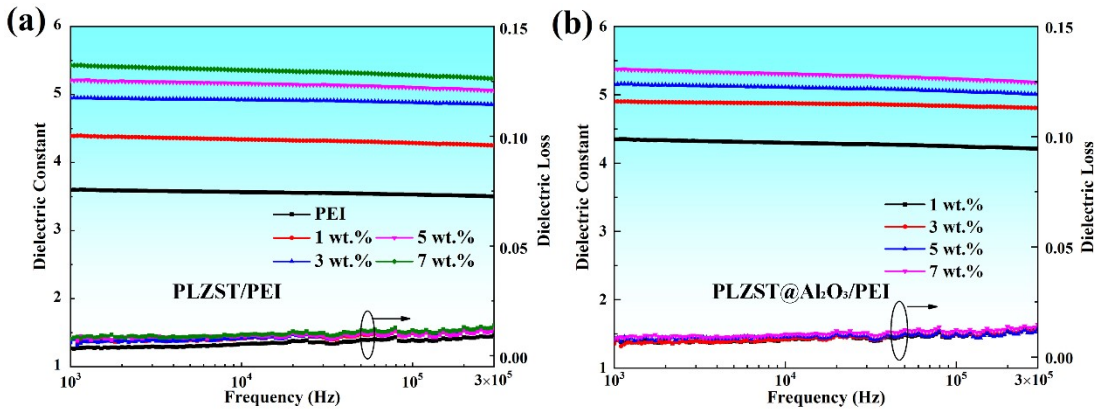

Fig. S10. Room-temperature frequency dependence of dielectric constant and loss of PEI nanocomposites loaded with various (a) PLZST and (b) PLZST@Al_2O_3 contents.

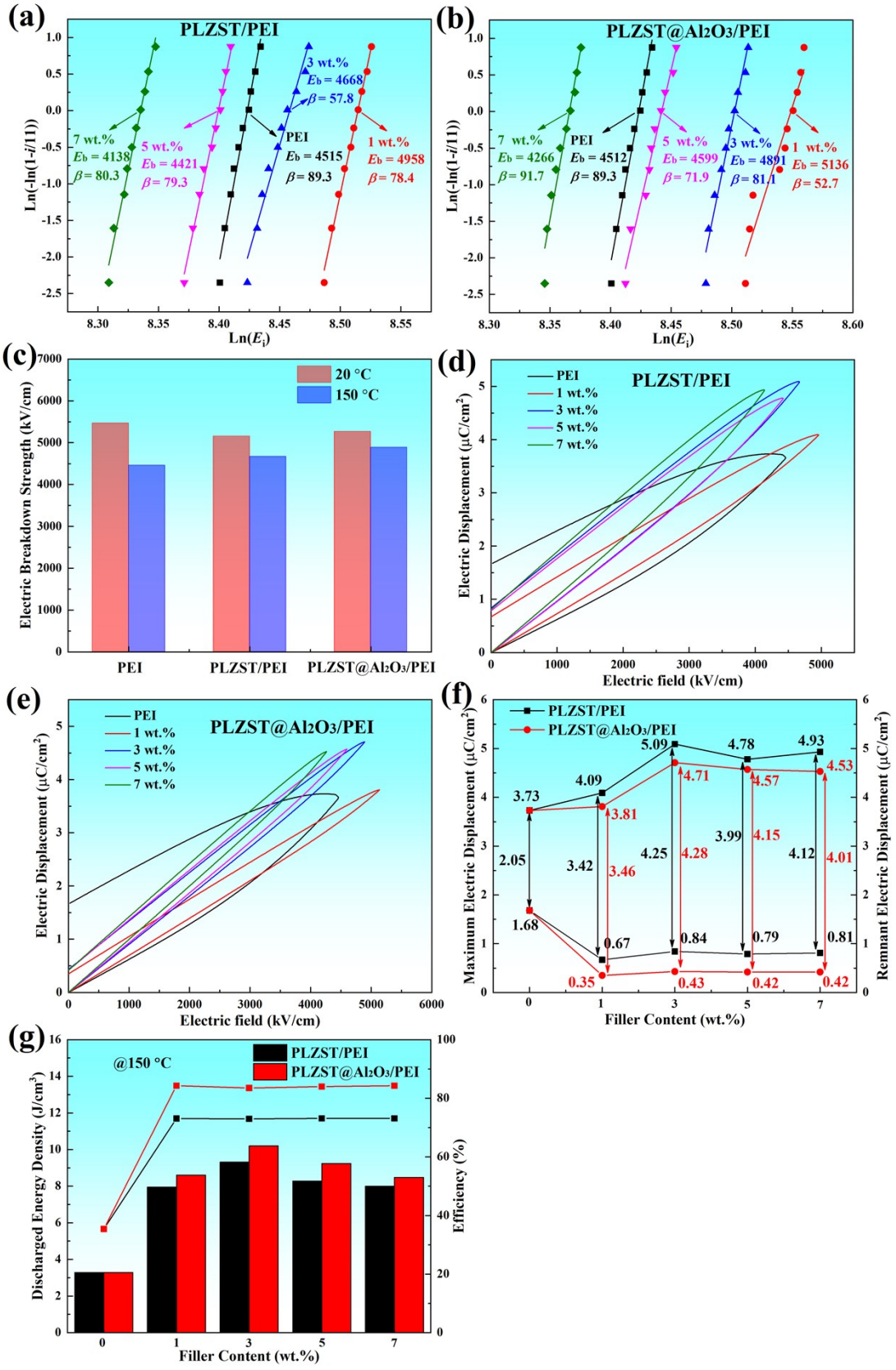

Fig. S11. Weibull distribution plots of PEI nanocomposites with various (a) PLZST and (b) PLZST@Al_2O_3 NP contents at 150 °C. (c) Comparison of E_b of PEI and PEI

nanocomposites with 3 wt.% PLZST and PLZST@Al_2O_3 NPs at 20 and 150 °C. *D-E* loops of PEI nanocomposites with various (d) PLZST and (e) PLZST@Al_2O_3 NP contents near the breakdown strength at 150 °C. (f) D_{max}, D_r, D_{max}-D_r, and (g) energy storage properties of PEI nanocomposites with various PLZST and PLZST@Al_2O_3 NP contents at 150 °C.

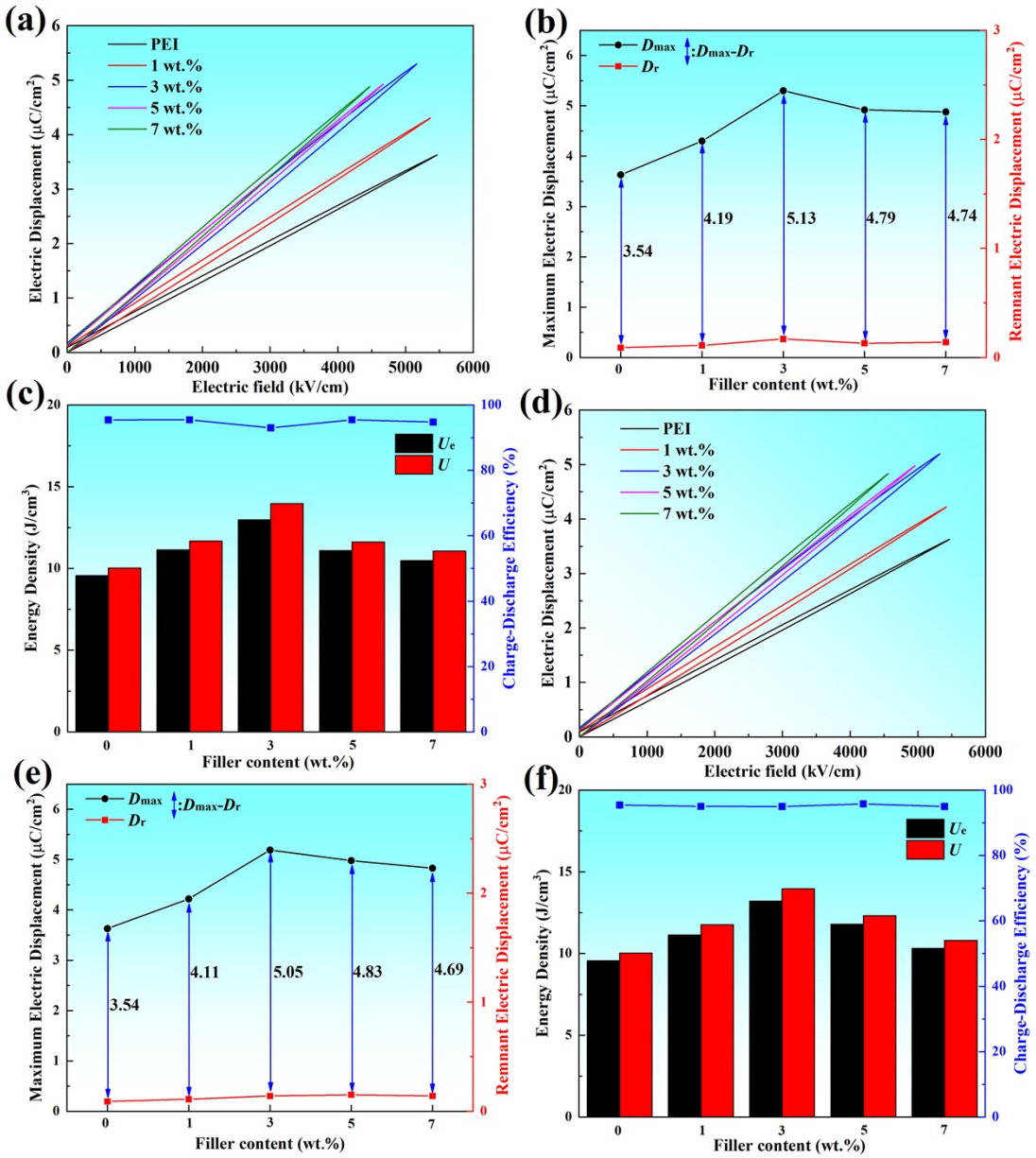

Fig. S12. Room-temperature (a) *D-E* loops near the breakdown strength, (b) D_{max}, D_r,

and D_{max}-D_r, and (c) energy storage properties of PEI nanocomposites with various PLZST NP contents. Room-temperature (d) *D*-*E* loops near the breakdown strength, (e) D_{max}, D_r, and D_{max}-D_r, and (f) energy storage properties of PEI nanocomposites with various PLZST@Al_2O_3 NP contents.

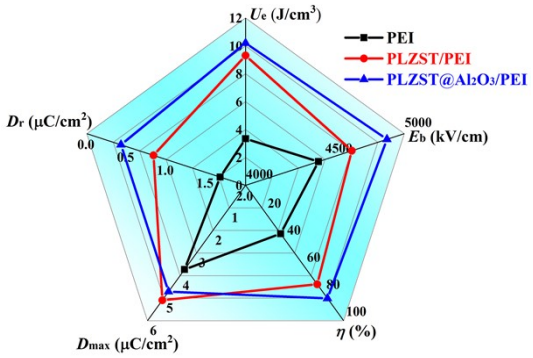

Fig. S13. Dielectric and capacitive parameters of PEI and PEI nanocomposites with 3 wt.% PLZST and PLZST@Al_2O_3 NPs at 150 °C.

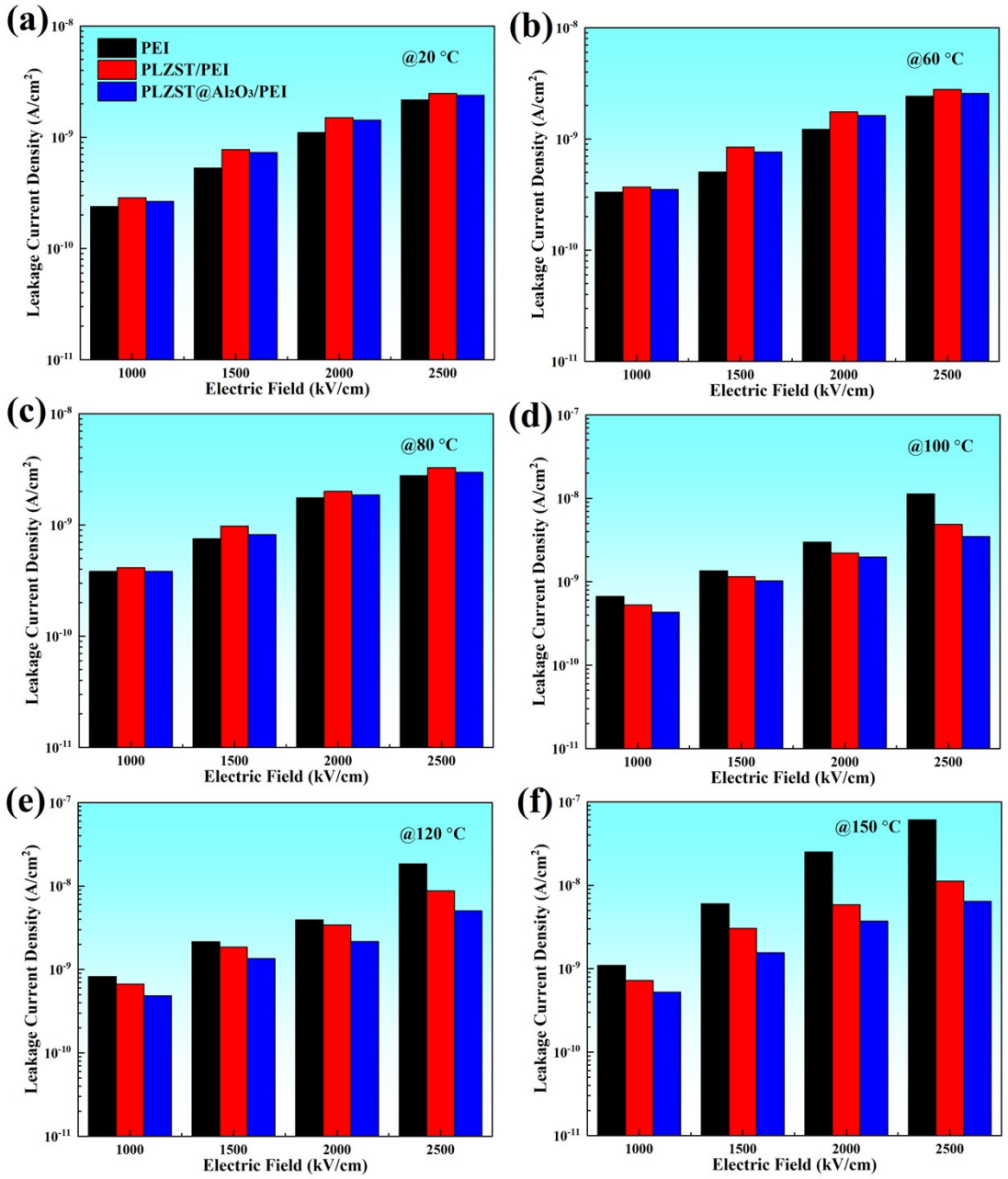

Fig. S14. Electric field dependence of the leakage current density of PEI and PEI nanocomposites with 3 wt.% PLZST and PLZST@Al_2O_3 NPs at (a) 20 °C, (b) 60 °C, (c) 80 °C, (d) 100 °C, (e) 120 °C and (f) 150 °C.

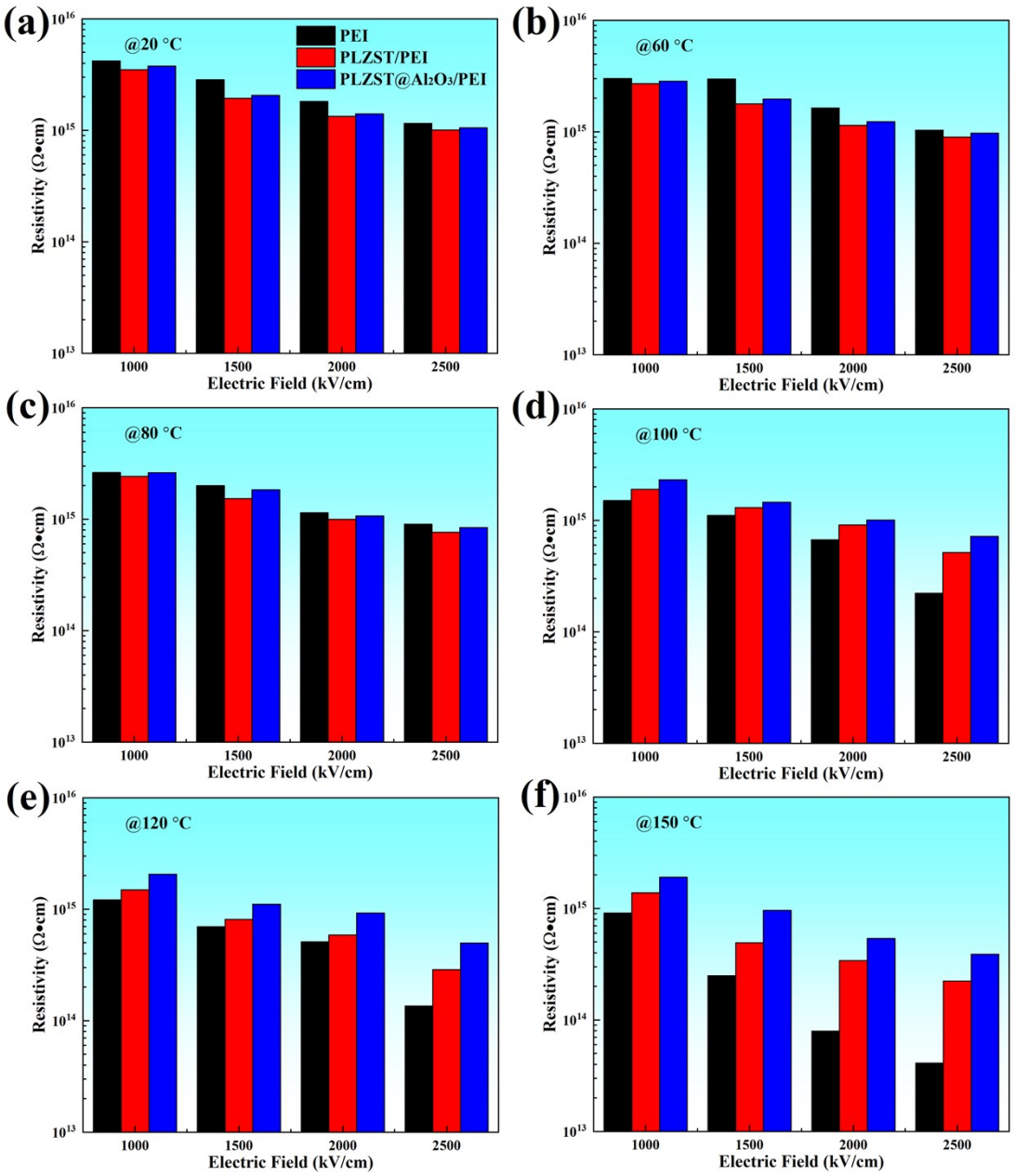

Fig. S15. Electric field dependence of the resistivity of PEI and PEI nanocomposites with 3 wt.% PLZST and PLZST@Al_2O_3 NPs at (a) 20 °C, (b) 60 °C, (c) 80 °C, (d) 100 °C, (e) 120 °C and (f) 150 °C.

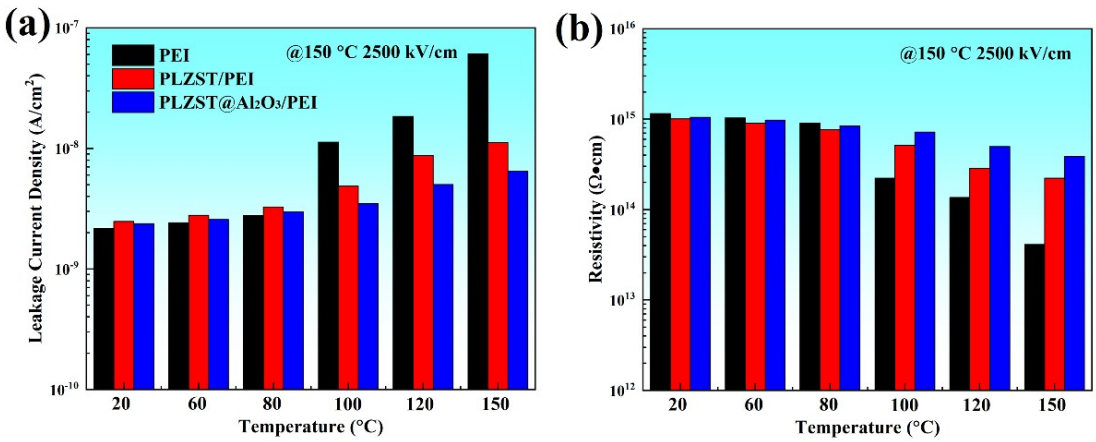

Fig. S16. (a)The leakage current density and (b) resistivity of PEI and PEI nanocomposites with different PLZST and PLZST@Al_2O_3NP contents measured at 2500 kV cm^{-1} and the temperature of 20-150 °C.

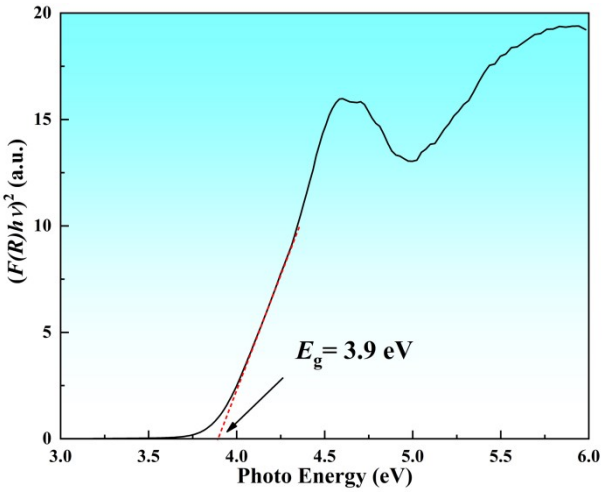

Fig. S17. [$F(R)hv)^2$] versus hv plots for the PLZST ceramic.